Details of HPM generation in atmospheric air using the laser and klystron terminology

Mladen M. Kekez

Abstract—**This study gives more details of the concept by Kekez [6-7] of the HPM generation by corona and spark channel discharges in atmospheric air. The paper offers approximate expressions regarding the frequencies that leave the cavity. The experimental data are given to illustrate the processes involved together with the effects of super-radiance.**

Index Terms— **HPM generation, klystron, resonant cavity, corona and spark channel discharges**

I. INTRODUCTION

Prishchepenko presented his findings (i.e. Ref [1]) at the EUROEM Conference held in Bordeaux, France in 1994 indicating the use of old-fashion explosively driven magneto-cumulative generator (MCG), invented in 1951 by A. D. Sakharov [i.e. Ref. 2], to drive a number of compact explosively driven RF/HPM munitions. The MCG is used as an energy converter needed to transform the chemical /mechanical energy of the explosion into the electrical energy impulse of RF/HPM frequencies. This concept indicates that a flash of high-power radio frequency (RF) or high-power microwave (HPM) radiation may burn any electronic circuit it hits.

The MCG's have extraordinary large reservoir of energy. See for example Ref. [3]. The energy density of an explosive is up to 5-6 orders of magnitude larger than the energy density stored in the condensers. The output voltage of up to 400 kV has been achieved by Sun *et al* [4] using electrically exploding switch in their small-size MCG capable of producing more than 20 GW into a 6 Ω resistive-load.

Chernyshev *et al* [5] have demonstrated that the increase of MCG power can be obtained by selecting the construction of foil opening switch, having the extended break surface. Using the condenser bank, they have achieved that the power transferred into the load was not lower than 420 kV, 10 MA, $20 \cdot 10^{12}$ W respectively. Further work of Chernyshev's group has raised the high power voltage pulse to 1 MV with the pulse width of 300 ns.

Kekez [6 and 7] has proposed the mechanism of the

M. M. Kekez is with High-Energy Frequency Tesla Inc., (HEFTI), 2104 Alta Vista Drive, Ottawa, Canada, K1H 7L8, (e-mail: mkekez@magma.ca, web: www.hefti.ca)

conversion of energy contained in the pulse coming from the MCG or the equivalent sources (i.e. Marx generator) into RF/HPM pulse. Existing laws in the field of laser and klystron science were applied in the formulation together with the laws of interaction between plasma/electron beams and the electromagnetic (radiation) wave. The present paper gives more details of this proposed mechanism for the HPM generation in atmospheric air.

II. EXPERIMENTAL SET-UP

Schematic of the experimental set-up is shown in Fig. 1. There are two differences between this arrangement and the one given in Ref [6]. The output post from the 9-stage Marx generator is enlarged (to be able to hold the helical antenna in the vertical position) and the helical antenna is placed on the post in the resonant cavity.

The helical structure is self-supporting in the vertical position. If any dielectric material is used to hold the structure in the vertical position, the FFT's data will be difficult to be understood.
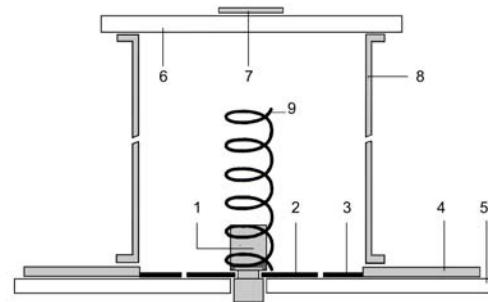
Figure 1; 1-HV output from the 9-stage Marx generator, 2–"hot" copper plate 3–"cold" copper ring, 4-ground flange of the generator, 5- and 6-plexiglass flanges, 7-partial reflector, 8-nipple, 9-helix. B-dot probe is placed above the partial reflector.

The separation between the "hot" copper plate, 2 and the "cold" copper ring, 3 of Fig.1 was varied between 1.5 mm and 3 mm. When the voltage impulse reaches the electrode 1 and the plate 2, the voltage impulse sees an open-circuit enabling the voltage to double its value for a very short period of time. The electric field in this gap is highly non-uniformed and is in MV/cm range. 9-stage Marx generator used is charged to 17.5 kV / stage. The energy stored in the generator is 21 Joules. B-dot probe is made by Advanced Engineering Manufacturing
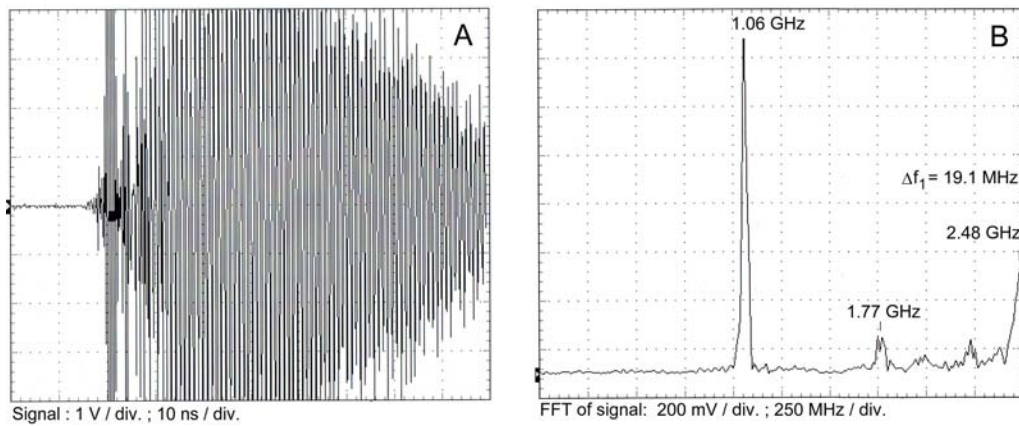
Fig.2 Signal is given in Frame A and FFT is given in Frame B.

Initially the system radiates at frequencies of 1.77 MHz and 2.48 MHz
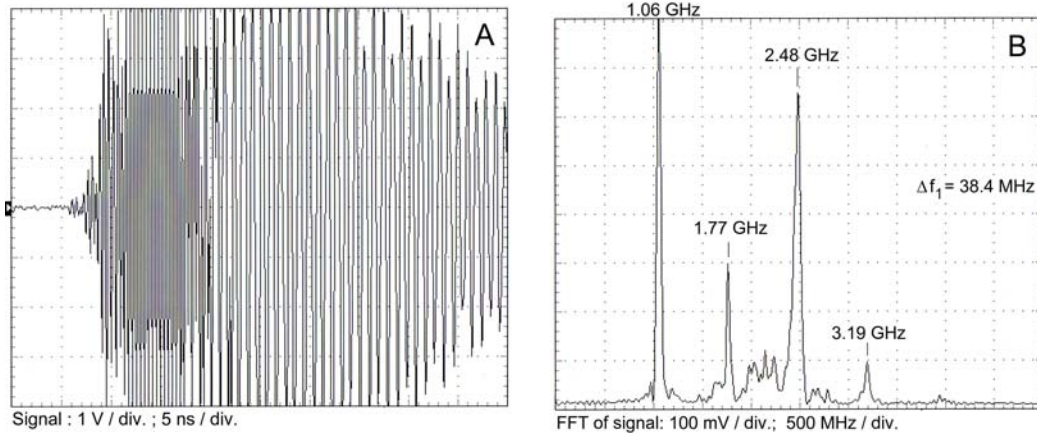
Fig. 3 Description as in Fig. 2.The signal is recorded on 5 ns /div. time scale

Later, the system radiates manly at frequency of 1.06 GHz
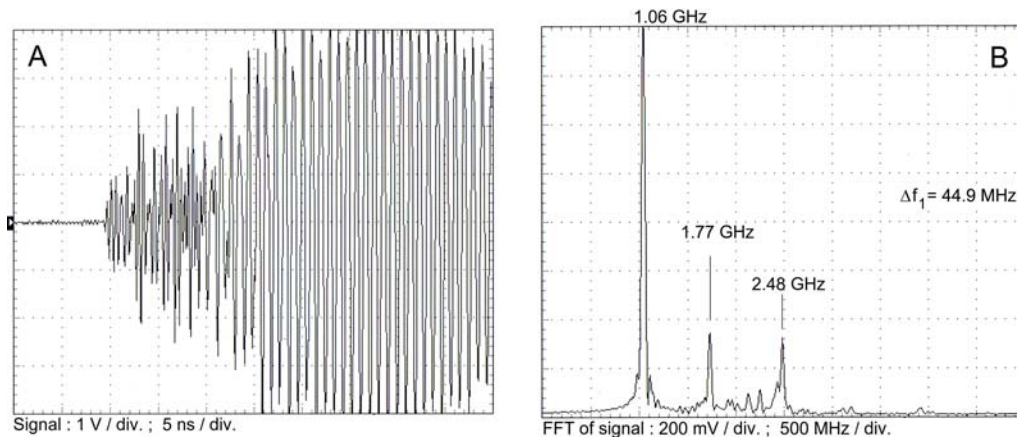
Fig. 4 Description as in Fig. 2. The signal is recorded on 5 ns /div. time scale.

Fig. 4 and Fig. 3 are recorded under the same experimental conditions

Solutions, Albuquerque, NM 87123, USA and is calibrated in the TEM-cell designed specifically to calibrate the sensors. For frequency of 1.06 GHz, the amplitude of the signal of 1 Volt corresponds to the electric field of 3.07 kV/cm.

III.   EXPERIMENTAL DATA

The experimental data are given in Figs. 2 to 6. The B-dot probe produces the signal with amplitude linearly proportional (rises) with the frequency applied. This fact makes the appearance of higher frequencies to be overstated in Figs. 2 to 4.

To illustrate this point let us consider Fig. 3, Frame B as an example. If the B-dot probe would have the frequency independent response, the amplitude at 1.77 GHz would be decreased by factor of 1.67 in respect to the frequency at 1.06 GHz and the amplitude at 2.48 GHz would fall by factor of 2.34 in respect to the frequency at 1.06 GHz.
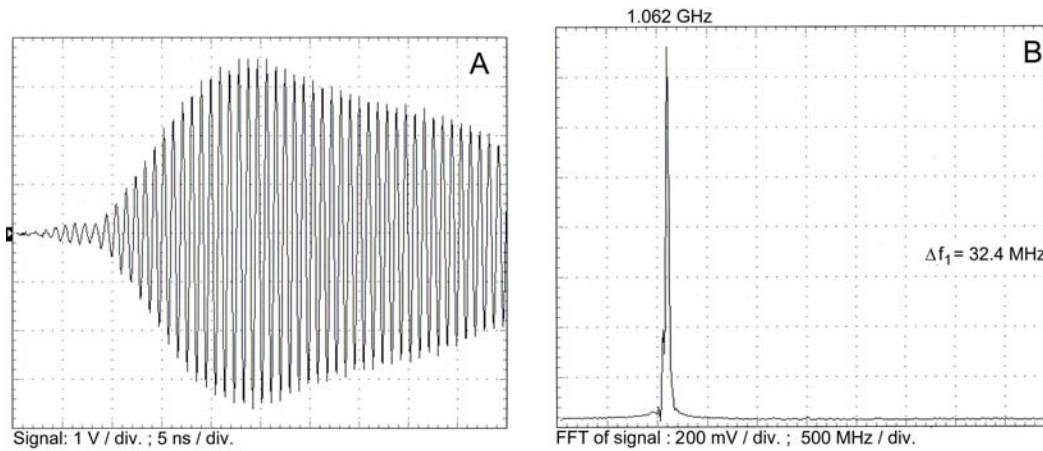
Fig.5 Description is as in Fig. 2. The signal is recorded with 1 GHz low pass filter. In Figs. 2 to 6 of FFT data, Δf_1 is the FWHM of 1 GHz radiation.

The waveform remains the same, when 1.25 GHz low pass filter has replaced 1 GHz low pass filter.

Further decrease in the amplitude of the frequencies above 1.06 GHz is expected when the additional waveguide with 1 GHz horn antenna are attached to the nipple, 8 of Fig.1 and the fields are measured in the far-field domain.

Variations in the shape of the pulse are observed from shot to shot. These variations are reflected in the amplitudes of the frequency spectra recorded in the FFT diagram. However, the frequency value in the FFT plot remains constant regardless how many shots are fired and how many runs are made. Only the heights of each frequency in the FFT may change as can be noted by comparing Fig. 3, Frame B with Fig. 4, Frame B. Also, the frequency difference between two adjacent lines remains constant and equal to 710 MHz

IV. DISCUSSION

The cut-off wavelength for the TE_{11} mode in the coaxial waveguide is:

$$\lambda_C = \frac{1}{2} \, 1.873 \, \pi \, (a+b) \qquad \text{when } a = 3b \qquad (1)$$

Here, a is the radius of the inner wall of the nipple (cylinder) and b is the radius of the circular conductor of the coaxial waveguide. The TE_{11} mode has the smallest cut-off frequency value for the coaxial waveguide.

For a=3"=7.62 cm, and b=1"=2.54 cm, Eq. 1 yields λ_C = 29.876 cm and f_c = 1.004 GHz. If the helical antenna can approximate the inner conductor of the coaxial waveguide, Eq. 1 is applicable for the set-up given in Fig. 1. Figs. 2 to 5 state that the dominant frequency is 1.06 GHz and Eq. 1 gives f_c to be 1.004 GHz.

When the helical antenna is absent, the frequency of 1.74 GHz was observed and it was the only frequency present in the cavity. The conditions were the semi-uniform distribution of the spark channels between the "hot" copper plate, 2 and the "cold" copper ring, 3. See Ref. [6]. When the dimensions of the hot plate and cold ring are changed, the frequency is also changed to read 2.01 GHz and it was the only frequency present in the cavity. This is also shown in Ref. [6].

The helical antenna was designed according to Kraus *et al* [8] with the pitch for the helical antenna close to $\lambda/4$ and the wavelength, λ of $2\pi b$. The antenna was made of ¼" (=0.635 cm) diameter copper tubing and it was coiled on 2" (=5.08 cm) diameter rod. These dimensions enable the frequency of the antenna to be 1.89 GHz.

Without the antenna, the velocity of the electromagnetic wave in the cavity is c (=3 10^8 m/sec.). With the antenna, the velocity of the wave is decreased approximately to:

$$v \approx c \, (\text{pitch} /(2\pi b))= c/4. \qquad (2)$$

Kraus *et al* [8] have also shown that near the open end of the helical antenna there are standing waves over a short distance. If we take that the distance, d of the single pitch at the end of the antenna follows the law of the simple spatial resonator: the round trip distance, 2d is equal to the integral number of wavelengths λ of the wave:

$$2d = N\lambda \quad \text{where N=\{ 1, 2, 3... \}} \qquad (3)$$

Eq. 3 for the distance, d of the single pitch is:

$$2* \text{pitch}=N\lambda$$

For these conditions, the resonant frequency, f_R describing the standing waves near the open end of the helix is:

$$f_R = Nc \,/(4\pi b) \qquad (4)$$

For N=1, and b= the inner radius of the helix=1" (=2.54 cm), Eq. 4 gives f_R = 940 MHz. For b= the outer radius of the helix = 1¼"(=3.175 cm), f_R = 752 MHz.

In the formulation the frequency f_R of Eq. 4 is added to the main emitting 1.06 MHz frequency line. This is in accord with Ref. [8, pp 224, their Fig. 8-3.b]. For comparison it should be noted that the frequency difference between two adjacent lines was measured to be 710 MHz, and this is of lower value in comparison to the value given by Eq. 4.

It should be noted that the envelope of the pulse in Fig. 5 is smooth compared to the envelopes given in Figs. 2 to 4. This indicates that the frequencies at 1.77 GHz, 2.48, GHz and 3.19
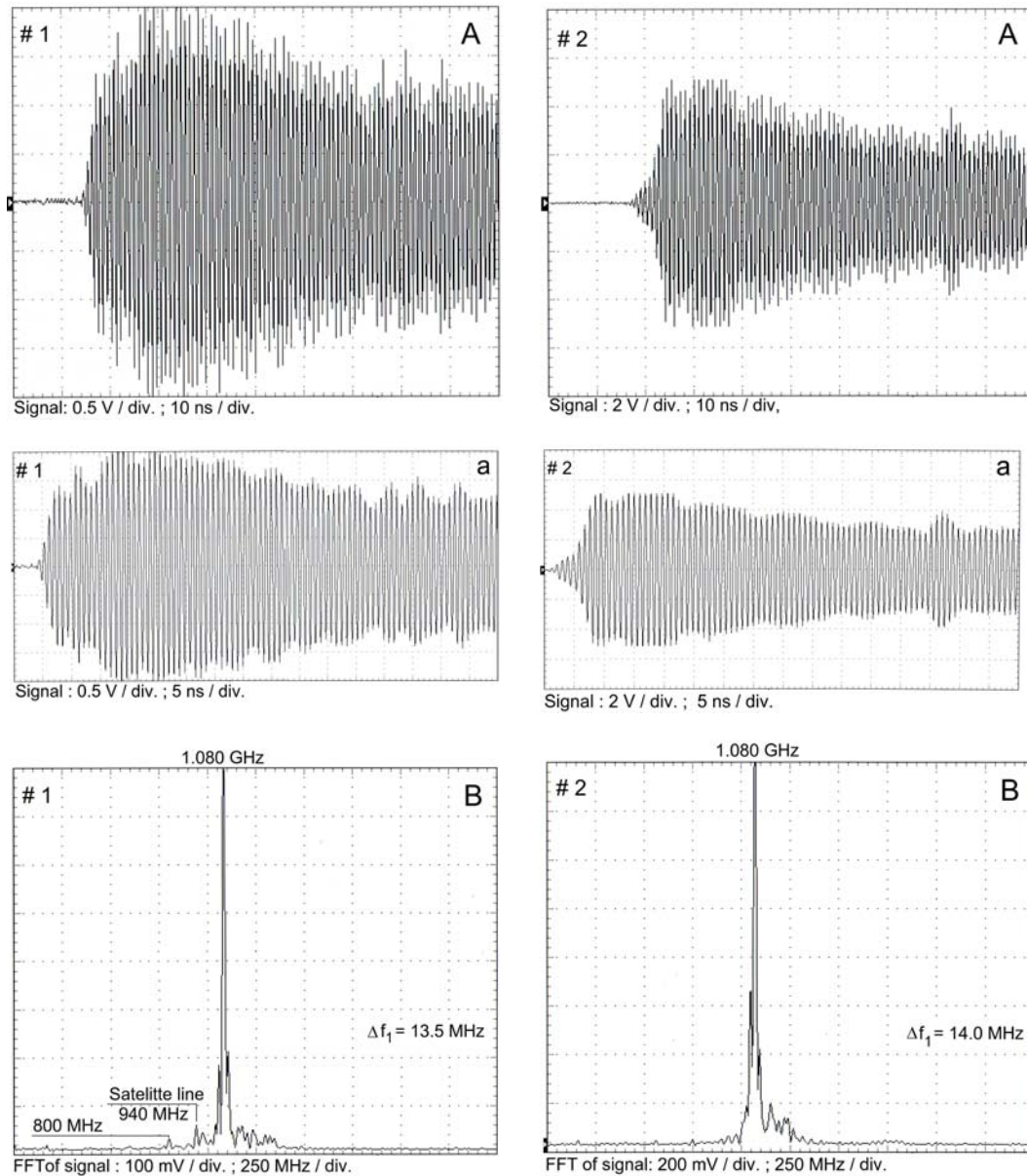
Fig 6 shows two shots: # 1 and 2 recorded when the system is tuned well. The signal is shown in frames A and a and FFT is given in frame B.

These figures also show the maximum amplitude variation from shot to shot. 1.25 GHz low pass filter is used. The records remain practically the same if 1.25 GHz low pass filter is absent.

GHz are continuously present during the main portion of the pulse.

We also need to consider the processes taking place in the space between the end of the helical antenna and the partial reflector. It should be stated that by minor adjustment of the position of the partial reflector and/or by increasing or decreasing the length of helical antenna by ¼ of a turn, the amplitude of the frequencies at 1.77 GHz and 2.48 GHz, shown in Fig. 2 and 4 can be reduced and instead of these frequencies we have many small amplitude (satellite) lines around 1.08 MHz. See Fig. 6

Figs. 2-5 offer the following picture. The cavity must be "pumped" first, before it can be "discharged". The Reltron tube by Miller et al [9] takes a few hundreds of nanoseconds to pump the cavity, before it starts to emit the radiation. In the present case the time difference between the pumping and discharging is short. Eq. 1 provides the main emitting frequency leaving the cavity.

It is not difficult to imagine that there are other possibilities by which the process of "pumping" and "discharging" of the cavity can occur. Here is an example.

In the study of super-radiance by Kekez [10], the set-up was similar to that of Fig. 1. For the super-radiance to occur, the condition is to have "strong" coupling. This means that the partial reflector is of relatively larger size (in comparison to the one used in Fig. 1) and is placed closer to the helix. With 100% mirror the strong electromagnetic (radiation) wave is formed as it bounces back and forth in the cavity gaining the strength from the energy being transferred from the high-speed electrons.

To understand the experimental data, the idea of Dicke's concept of super-radiation [11] is adopted. It is assumed that this concept (related to the atoms) can be applied to the high-speed electrons: i.e., the electrons are grouped together by their common radiation field and the intensity emitted by N high-speed electrons is proportional to N^2 instead of N.

The second assumption is that for the incoming electro-magnetic (radiation) wave will cause the high-speed electrons to be bunched. Plasma maintains approximate charge neutrality and the electrostatic forces in plasma (represented by plasma frequency) will oppose the bunching process. Therefore, the plasma frequency dictates the period of time for the energy transfer from high-speed electrons to the electromagnetic (radiation) wave. With these two assumptions, the experimental (and theoretical) data are summarized as:

$$\text{Energy content in the pulse} = \text{constant} / (\Delta t)^3 \qquad (5)$$

where Δt is the full width at half magnitude (FWHM) of the electric field signal on power 2

It should be noted that in contrast to Dicke's concept, the frequency of radiation in the microwave field is governed by the size of the cavity (and by the slow wave structure, SWS when BWO is used). If the cavity is not tuned well, the system will have the spectral bandwidth, Δf_1 and the system will experience the coherence phenomenon that is causing the pulse shortening of the HPM pulse. See Ref. [12].

It is now confirmed by the author that the coherence phenomenon of Ref [12] is also dictating the duration of super-radiance pulse and it explains why the pulse is of short duration. When Δf_1 is reduced, it is possible to get the super-radiance pulse of longer duration.

To achieve "strong" coupling and get the super-radiance pulse, Eltchaninov *et al* [13] have placed both the antenna and the cathode at one end of the SWS and the 100% reflective mirror is placed at the other end of their BWO's. This way, the cavity is "pumped" hard and for longer period of time, in comparison to the classical BWO system (where the cathode is at one end of the SWS and the antenna is at the opposite site of the SWS). Unfortunately, Eltchaninov *et al* have not stated Δf_1 of the pulses recorded, so we cannot fully appreciate their data.

V. CONCLUSIONS

The experimental set-up shown in Fig. 1 has some common points with the Vircator arrangement of Kitsanov *et al* presented in Ref [14]. It appears to the author that in Kitsanov *et al* experimental work, the double mesh or double foils were used also to ensure that the radiation produced by the pulse generator do not enter the resonant cavity and be one of the component causing unwanted "chirping" of the frequency being generated by the system. In the present arrangement the dimensions of the "hot" and "cold" plate are chosen to be as such to allow the minimum penetration of unwanted frequencies from the generator into the cavity.

The helical antenna is introduced in the resonant cavity to mitigate the effects of the uneven distribution of the spark channels occurring between the "hot" and "cold" plate/ring. The antenna enables the reliable coupling (i.e., "highway" of the wave propagation) between the partial reflector and 100% reflector composed of the plate/ring. This set-up eliminates the "chirping" and suppresses the pulse-shortening processes that is hampering the HPM research for some time.

When argon at high pressure had replaced air in similar experiment set-up, further improvements have been observed. The variations in the HPM amplitude have been suppressed and the HPM emissions have been enhanced. These findings are easy to be understood. In the rail spark gap studies, it is well known fact that with argon present in the gas mixture, the number of spark channels per unit length is increased, leading to smaller overall inductance in the circuit and higher current.

Further work is needed to confirm these findings at higher energy levels: 0.1 MA at 0.5 MV. The question still remains whether it is necessary to introduce the dielectric lens to replace the plexiglass flange, 6 shown in Fig. 1 to accomplish more efficient energy extraction from the cavity.

REFERENCES

[1] A. B. Prishchepenko, "Devices built around permanent magnet for generating an initial current in helical explosive magnetic generators", *Instruments and Experimental Techniques*, **38**, p 515-520, 1995

[2] A. D. Sakharov, "Magneto implosive generators", *Sov. Phys. Uspekhi*, **9,** p 294-299, 1966

[3] A.Ya. Brodskii, V. A. Vdovin, A. V. Korzhenevskii, A. S. Kravchenko, A. I. Pavlovskii, V. D. Selemir, S. A. Sokolov, V. A. Cherepenin and Z. S. Chernov "Conversion of explosive energy into electromagnetic radiation in the microwave region" *Sov. Phys. Dokl*. **35,** p 876-877, 1990

[4] Q. Sun, C. Sun, X. Gong, W. Xie, S. Hao, Z. Liu, W. Dai, Y. Chi, W. Liu, M. Wang, N. Zhang and W. Han, "High-power and high-voltage pulse generation on resistance load by means of EEMGS" *Proc. 10th Int. Conf. on Megagauss Field and Related Topics,* Berlin, Germany, p. 201–206, July 2004.

[5] V. K. Chernyshev, A.I Kucherov, A. B. Mezhevov, A. A. Petrukhin, and V. V. Vakhrushev, "Electro-explosive foil 500 kV current opening switch characteristics research", *Proc. 11th IEEE Conf. on Pulsed Power,* Baltimore, USA, p. 1208-1212, June 1987

[6] M. M. Kekez, "Description of HPM generation in atmospheric air using the laser and klystron terminology", *(to be published in IEEE Trans Plasma Sci.)*

[7] M. M. Kekez, "HPM generation in atmospheric air", *Proc. the 13 Int. Conf. on Megagauss magnetic field generation and related topics*, Suzhou, China, 2010

[8] J. D. Kraus J. D and R. J. Marhefka, *Antenna for all applications*, *Third Edition*, McGraw Hill-Boston, 2002

[9] R. B. Miller, W.F. McCullough, K. T. Lancaster and C.A. Muehlenweg, "Super-reltron theory and experiments", *IEEE Trans. Plasma Sci.,* **20**, p 332-343, 1992

[10] M. M. Kekez, "HPM super-radiance in atmospheric air", *Proc. the 13 Int. Conf on Megagauss magnetic field generation and related topics,* Suzhou, China, 2010

[11] R Dicke, "Coherence in spontaneous radiation processes", *Phys. Rev*. **93,** pp 99-110, 1954

[12] M M Kekez, "Coherence of HPM generation in air" *(to be published in IEEE Trans. Plasma Sci., see also http://www.hefti.ca/)*

[13] A A Eltchaninov, S D Korovin, G A Mesyats, I V Pegal V V Rostov V G Shpak and M I Yalandin, "Review of studies of superradiative microwave generation in X band and Ka band relativistic BWO's", *IEEE Trans. Plasma Sci.,* **32**, pp 1093- 1099, 2001

[14] J. Benford, J. A. Swegle and E. Schamiloglu, *High Power Microwaves*, Second editions, *(NY; Taylor & Francis Group),* 2007

BIOGRAPHY: (NOT AVAILABLE)